JOC The Journal of Organic Chemistry

Article

pubs.acs.org/joc

Diastereomer Configurations from Joint Experimental–Computational Analysis

Abil E. Aliev,* Zakirin A. Mia, Mathilde J. M. Busson, Richard J. Fitzmaurice, and Stephen Caddick

Department of Chemistry, University College London, 20 Gordon Street, London WC1H 0AJ, U.K.

Supporting Information

ABSTRACT: The potential of the approach combining nuclear magnetic resonance (NMR) spectroscopy, relaxed grid search (RGS), molecular dynamics (MD) simulations, and quantum mechanical (QM) calculations for the determination of diastereomer configurations is demonstrated using four diastereomers of a trisubstituted epoxide. Since the change in configuration of the chiral center is expected to change the distribution of conformer populations (including those of side-chain rotamers), changes in NMR parameters [chemical shifts, *J* couplings, and nuclear Overhauser effects (NOEs)] are expected. The method therefore relies on (1) identification of possible conformations in each diastereomer using relaxed grid search analysis and MD simulations; (2) geometry optimizations of conformers selected from step (1), followed by calculations of their relative energies (populations) using QM methods; (3) calculations of averaged NMR parameters using QM methods; (4) matching calculated and experimental values of NMR parameters of diastereomers. The diastereomer configurations are considered resolved, if three NMR parameters different in nature, chemical shifts, *J* couplings, and NOEs, are in agreement. A further advantage of this method is that full structural and dynamics characterization of each of the diastereomers is achieved based on the joint analysis of experimental and computational data.

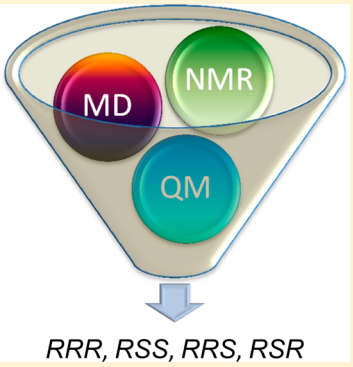

1. INTRODUCTION

One of the difficult structural problems in NMR spectroscopy is the determination of the configuration of diastereomers.[1] Theoretically, the change in the absolute configuration of one of the chiral centers is expected to change the distribution of conformer populations (including those of side-chain rotamers and ring conformations), which in turn is expected to lead to changes in NMR parameters. In practice, however, there are usually a large number of possible conformers, and it is impossible to predict their populations in advance without a detailed computational analysis. The accuracy of quantum mechanical (QM) methods in predicting relative energies (populations)[2] and NMR parameters[3,4] of conformers has considerably improved in recent years. Therefore, averaged NMR parameters can be predicted for various combinations of absolute configurations in compounds with two or more chiral centers using QM methods. Comparison of the computed and experimentally measured values of NMR parameters is expected to distinguish diastereomer configurations, and such a joint analysis has been undertaken in this work.

Four diastereomers of a trisubstituted epoxide **1** were considered (Figures 1 and 2).[5] The absolute configuration of the C3 atom of the five-membered ring was known in advance (3*R*; note: arbitrary atom numbering is used). This leaves four possible combinations of *R*- and *S*-configurations for chiral centers C8 and C10, which are shown in Figures 1 and 2. In two of them, the two alkynes are in a *cis*-configuration (denoted as **c1** and **c2**), whereas in the other two, they are in a *trans*-configuration (denoted as **t1** and **t2**). While discrimination between *cis*- and *trans*-configurations is relatively easy, distinguishing **t1** from **t2** or **c1** from **c2** is not straightforward. For example, the conformation of the five-membered dioxolane is likely to change from one diastereomer to another, which in turn is likely to affect the population of rotamers about the C3–C8 bond. Herein, we show that the joint experimental–computational analysis is capable of addressing this issue without a need for crystallographic measurements. An additional advantage of this approach is that full structural and dynamics characterization of each of the diastereomers is achieved based on the joint analysis of experimental and computational data.[6]

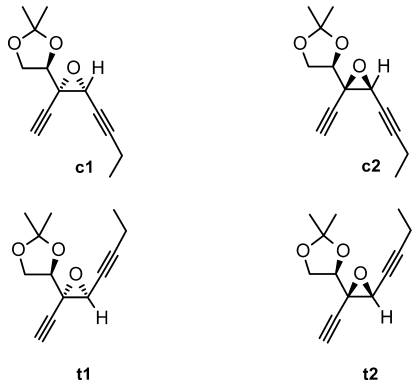

Figure 1. Schematic presentation of four possible diastereomer structures of **1**.

Received: June 5, 2012
Published: June 26, 2012

   dx.doi.org/10.1021/jo301119h | *J. Org. Chem.* 2012, 77, 6290–6295

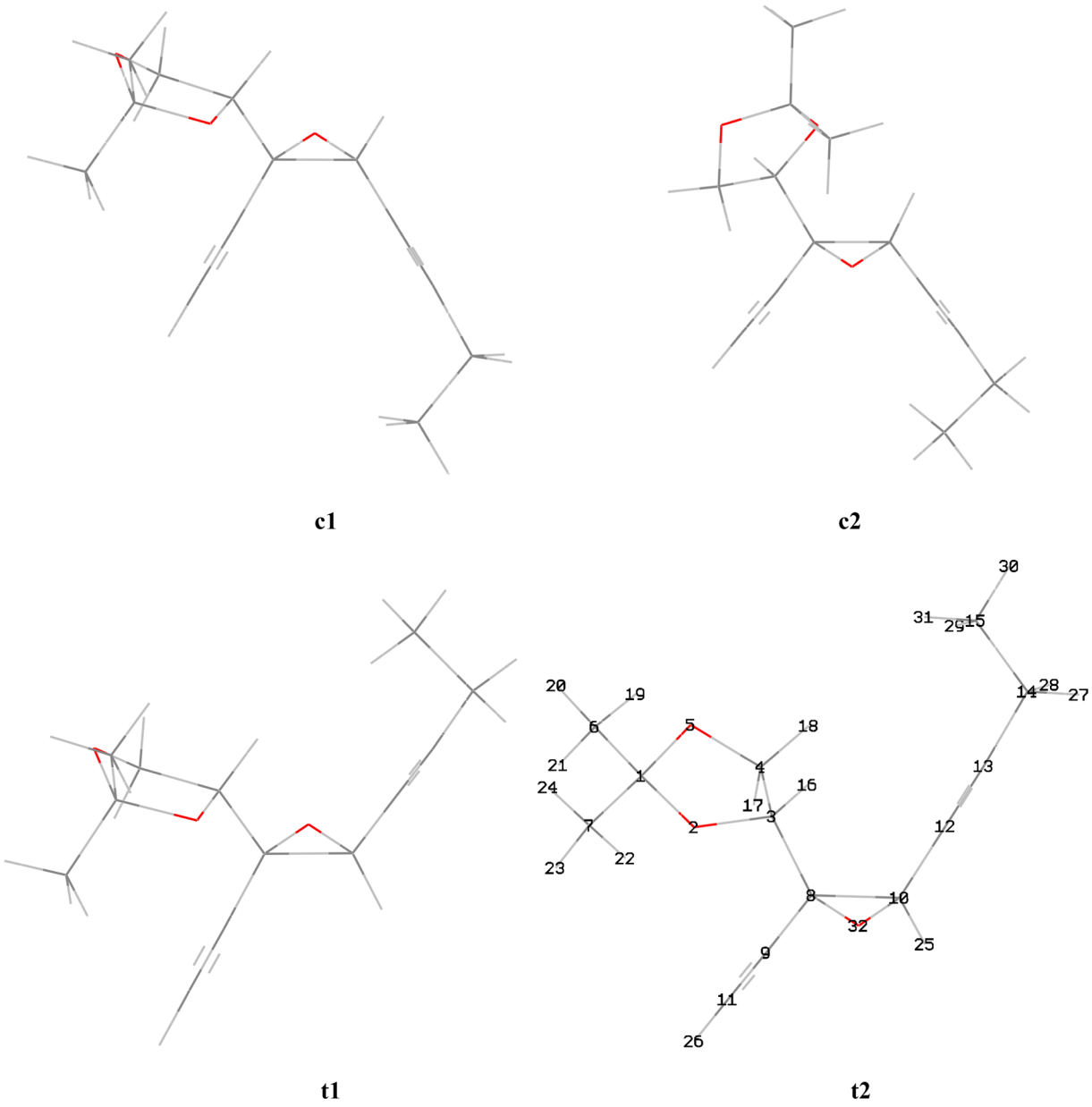

Figure 2. Lowest-energy geometries of the *cis*- (**c1** and **c2**) and *trans*-isomers (**t1** and **t2**) of **1** from the relaxed grid search analysis, together with the atom numbering used (shown for **t2**). In **c1** and **t1**, the O atom (red) of the three-membered ring is placed at the back of the C−C bond in the same ring. In **c2** and **t2**, the O atom of the three-membered ring is placed in front of the C−C bond in the same ring. The configurations are 3*R*,8*S*,10*R* in **c1**; 3*R*,8*R*,10*S* in **c2**; 3*R*,8*S*,10*S* in **t1**; and 3*R*,8*R*,10*R* in **t2**.

2. RESULTS AND DISCUSSION

One of the diastereomers of **1** was available in a pure form (**1a**), whereas three others (**1b**, **1c**, and **1d**) were only isolable as a mixture. The ^{1}H NMR spectrum of the mixture of three diastereomers showed three distinct peaks for H25; thus, the ratio of isomers, 4.0:1.3:1.0 (**1b**:**1c**:**1d**), could readily be determined by integration (Figure S1 of the Supporting Information). Except for the known *R*-configuration of the C3 atom, the configurations of chiral centers, C8 and C10, were unknown.

The *cis*- and *trans*-configurations of the two epoxy−diyne pairs were determined by evaluation of the ^{3}J (C9,H25) coupling in each diastereomer. Since the three-membered ring has a rigid geometry, the dihedral angle H25−C10−C8−C9 is ∼0° in **t1** and **t2** and ∼120° in **c1** and **c2**. Therefore, based on the expected Karplus-type relationship for $^{3}J_{CH}$ couplings,[7] the value of ^{3}J (C9,H25) is likely to be smaller in *cis*-isomers compared to *trans*-isomers. The predicted values of these coupling constants, determined using the lowest-energy geometries of the *cis*- (**c1** and **c2**) and *trans*-isomers (**t1** and **t2**) of **1** from the RGS analysis (Figure 2) at the B3LYP/6-311+G(2d,p) IEFPCM-($CHCl_3$) level of theory, were 0.27 Hz (**c1**), 0.41 Hz (**c2**), 2.10 Hz (**t1**), and 2.40 Hz (**t2**). Additional B3LYP/EPR-III IEFPCM($CHCl_3$) calculations of *J* couplings were also carried out, and the predicted values of ^{3}J (C9,H25) coupling constants at the B3LYP/EPR-III level were 0.40 Hz (**c1**), 0.56 Hz (**c2**), 2.21 Hz (**t1**), and 2.55 Hz (**t2**), which are in good agreement with the results from B3LYP/6-311+G(2d,p) calculations.

The experimental values of the ^{3}J(C9,H25) coupling were determined from the proton-coupled ^{13}C NMR spectra, which were 0.92 Hz (**1a**), 2.20 Hz (**1b**), 0.93 Hz (**1c**), and 2.43 Hz (**1d**). Based on the Karplus-type relationship between $^{3}J_{CH}$

dx.doi.org/10.1021/jo301119h | *J. Org. Chem.* 2012, 77, 6290−6295

couplings and the dihedral angle (H25−C10−C8−C9 in this case), as well as the predicted values from B3LYP calculations, relatively small values of the ^3J(C9,H25) coupling (~0.9 Hz) in **1a** and **1c** are in favor of the *cis*-configuration of the two triple bonds. Similarly, larger values of the ^3J(C9,H25) coupling (~2.3 Hz) in **1b** and **1d** indicate the *trans*-configuration of the two triple bonds.

A detailed analysis of possible conformers of each diastereomer of **1** is needed in order to distinguish between the two *cis*- and *trans*-configurations (i.e., between **c1** and **c2** or **t1** and **t2** configurations). The relaxed grid search was used initially to identify the most likely rotamers for each diastereomer **c1**, **c2**, **t1**, and **t2**. From the RGS analysis, three possible conformations were identified for each of diastereomers **c1** and **c2**, denoted as **c1a**, **c1b**, and **c1c** and **c2a**, **c2b**, and **c2c**, respectively (Figures S2 and S3 of the Supporting Information). Five (**t1a**−**e**) and seven conformations (**t2a**−**g**) were found for **t1** and **t2**, respectively (Figures S4 and S5 of the Supporting Information).

The main disadvantage of the RGS analysis is that the treatment of cyclic systems is difficult since bond rotations are limited due to constraints of the ring closure. MD simulations are capable of overcoming this limitation. Additional 5 μs long MD simulations at 298 K were, therefore, carried out for each diastereomer of **1**. Distributions of two dihedral angles, χ_1 = O2−C3−C8−O32 and χ_2 = O2−C3−C4−O5, and two interatomic distances, d_{CC} = C7...C15 and d_{HH} = H16...H25, were used to identify conformations for each of the diastereomers **c1**, **c2**, **t1**, and **t2** (Figures S6−S9 of the Supporting Information). Initially, the dihedral angle, χ_3 = C8−C10−C14−C15, was also examined. However, due to nearly flat χ_3 distributions (Figures S6−S9 of the Supporting Information), no attempt was made to distinguish conformers based on this angle. Ramachandran-type histograms for different combinations of χ_1, χ_2, and d_{CC} were also considered. An example of the (χ_1, χ_2)-histogram revealing the presence of four conformations in **t1** is shown in Figure 3. Based on the analysis of one- and two-dimensional

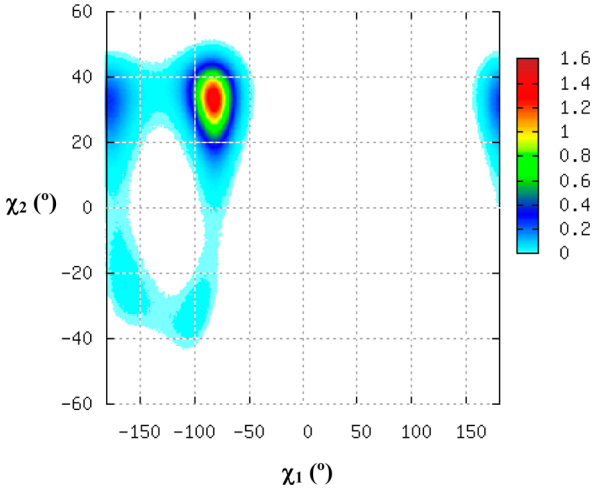

Figure 3. Ramachandran-type 2D histogram for χ_1 = O2−C3−C8−O32 and χ_2 = O2−C3−C4−O5 dihedral angle distributions in the MD GAFF simulation of **t1**.

(1D and 2D, respectively) histograms, several structures with distinct values of χ_1, χ_2, and d_{CC} were extracted from MD trajectories, and together with the results from the relaxed grid search analysis a total number of 54 structures of **1** were selected (13 structures of **c1** and **t1**, 14 structures of **c2** and **t2**). Geometry optimizations and frequency calculations were then carried out for all 54 structures using M06-2X/6-31G(d,p) IEFPCM($CHCl_3$) calculations.

The final optimized geometries, their relative energies, and estimated populations are included in Figures S2−S5 and Table S1 of the Supporting Information. For each of the structures, NMR parameters, spin−spin couplings and chemical shifts, were calculated at the B3LYP/6-311+G(2d,p) level of theory using M06-2X/6-31G(d,p)-optimized geometries. The M06-2X/6-31G(d,p)-predicted populations of conformers were used in calculating the averaged values of NMR parameters for each diastereomer. The calculated averaged ^3J(C10,H16) values were 3.93, 1.00, 3.19, and 0.70 Hz in diastereomers **c1**, **c2**, **t1**, and **t2**, respectively (Table S2 of the Supporting Information), which are in good agreement with the experimentally measured values of 3.70, 1.36, 2.80, and 1.32 Hz in diastereomers **1a**, **1c**, **1b**, and **1d**, respectively. Furthermore, the calculated values of ^{1}H and ^{13}C NMR chemical shifts (Tables S3 and S4 of the Supporting Information) were also in good agreement for the **c1**/**1a**, **c2**/**1c**, **t1**/**1b**, and **t2**/**1d** pairs. In particular, the largest ^{1}H NMR chemical shift difference in diastereomers **1a** and **1c** with the *cis*-configuration of two triple bonds is observed for H16: 4.05 ppm in **1a** and 4.30 ppm in **1c**. The predicted values at the B3LYP/6-311+G(2d,p) IEFPCM($CHCl_3$) level were 4.05 ppm in **c1** and 4.33 ppm in **c2**. Similarly, the experimentally observed configuration dependence of the ^{13}C NMR chemical shifts for C3 in diastereomers **1b** (75.20 ppm) and **1d** (78.15 ppm) with the *trans*-configuration of two triple bonds is reproduced by the B3LYP/6-311+G(2d,p) IEFPCM($CHCl_3$) calculations: 75.53 ppm in **t1** and 79.20 ppm in **t2**. Thus, the independent assignments of diastereomers relying on $^3J_{CH}$ couplings and chemical shifts are in agreement.

Based on NOE measurements, selective irradiation of the signal due to proton H25 leads to enhancements of the signal due to H16 by 1.0 ± 0.1% in **1a**, 0.1 ± 0.1% in **1b**, 0.5 ± 0.1% in **1c**, and 0.1 ± 0.1% in **1d**. Thus, the experimentally measured ratio of NOEs is 10:5:1:1 for **1a**:**1c**:**1b**:**1d**. In order to assign diastereomers, we need to estimate the expected values of conformationally averaged NOEs in diastereomers **c1**, **c2**, **t1**, and **t2** with known configurations (Figures 1 and 2). This in turn requires knowledge of the distance between protons H16 and H25 in each conformer of each diastereomer, as well as relative populations of each conformer. For both parameters, we rely on the M06-2X/6-31G(d,p)-predicted values (shown in columns 3 and 9 of Table S1 of the Supporting Information), the satisfactory accuracy of which has been confirmed previously.[6c,21,23] Assuming a simple r^{-6} dependence of NOEs (where r is the distance between protons),[8] averaged values of NOEs can then be calculated for each diastereomer as $\sum p_i r_i^{-6}$, where p_i is the population of conformer i and r_i is the distance between protons H16 and H25 in conformer i (for full details of NOE calculations based on QM data, see section 4.4). The calculated ratio is 6:3:1:1 for **c1**:**c2**:**t1**:**t2**, which is in agreement with the assignment of diastereomers based on J couplings and chemical shifts as **1a** = **c1**, **1c** = **c2**, **1b** = **t1**, and **1d** = **t2**, since the experimentally measured ratio of NOEs is 10:5:1:1 for **1a**:**1c**:**1b**:**1d**. However, it must be noted that diastereomers **1b** and **1d** cannot be distinguished based on NOE measurements alone, as the experimentally measured ratio of NOEs for these two diastereomers is 1:1.

To conclude, the analysis based on four different NMR parameters, $^3J_{CH}$ couplings, ^{1}H chemical shifts, ^{13}C chemical shifts, and NOEs, confirms that the configurations of C8 and C10 in diastereomers **1a**, **1b**, **1c**, and **1d** correspond to those of **c1** (3*R*,8*S*,10*R*), **t1** (3*R*,8*S*,10*S*), **c2** (3*R*,8*R*,10*S*), and **t2** (3*R*,8*R*,10*R*), respectively.[9]

dx.doi.org/10.1021/jo301119h | J. Org. Chem. 2012, 77, 6290−6295

3. CONCLUDING REMARKS

Since NMR spectroscopy provides a large pool of data such as chemical shifts of various nuclei, homo- and heteronuclear J couplings over a different number of bonds, and NOEs, it is most likely that at least some of these parameters will exhibit significant changes upon changing the configuration of diastereomers, despite their structural similarity. The analysis of data of different physical origin, therefore, increases the reliability of the configuration assignments based on the joint analysis of experimental and computational data. In particular, for four diastereomers of **1** considered in this work, three NMR parameters different in nature, chemical shifts, J couplings, and NOEs, were in full agreement in predicting diastereomer configurations. The use of more stringent criteria, relying on three NMR parameters different in nature, is justified for conformationally heterogeneous systems, such as diastereomer **c1** (**1a**), for which there is no single predominant conformer and the QM-predicted populations of the most abundant 12 conformers vary between 5 and 11% (see Table S1 of the Supporting Information).

The results also confirm that the accuracy of computational methods in predicting the relative stability of various possible conformational states, their geometry, and NMR parameters (^{1}H and ^{13}C chemical shifts and $^3J_{CH}$ couplings in this work) is satisfactory for successful stereochemical applications. These methods, combined with the experimental NMR data, offer a useful alternative to X-ray and neutron diffraction techniques.

4. EXPERIMENTAL SECTION

4.1. NMR Measurements. Solution ^{1}H NMR spectra were recorded on a 600 MHz NMR spectrometer equipped with a 5 mm cryoprobe (^{1}H 600.13 MHz and ^{13}C 150.90 MHz). Data acquisition and processing were performed using standard TopSpin (version 2.1) software. ^{1}H and ^{13}C chemical shifts relative to TMS were calibrated using the residual solvent peak (^{1}H 7.26 ppm and ^{13}C 77.15 ppm in $CDCl_3$).[10] Uncertainties in measured values of ^{1}H and ^{13}C chemical shifts are typically ±0.01 ppm. All spectra were recorded at 298 K.

Spin−spin couplings $^3J_{CH}$ were measured using proton-coupled ^{13}C spectra and selective heteronuclear 2D J-resolved (^{1}H, ^{13}C) spectra with an estimated uncertainty better than ±0.05 Hz (Figure S10 of the Supporting Information).[11] NOE measurements (with an estimated uncertainty of <0.1%) were undertaken for establishing spatial proximities of protons using a standard 1D NOESY sequence.[12]

4.2. Molecular Mechanics Calculations. Relaxed grid search (RGS) analysis[13] was carried out for each diastereomer of **1** using PCMODEL (version 8.5).[14] RGS is a systematic method, which involves creation of a large number of starting configurations and mapping out the shape of the potential energy surface. In this method the rotatable bonds of interest are first identified. The calculation starts by evaluating the energy when all the rotatable bonds are set to 180°. The bonds are then rotated sequentially, and all the structures are minimized and sorted based on their total energy, with any duplicate configurations removed. Since the total number of energy evaluations can be very large (usually several hundreds or thousands depending on the number of rotatable bonds), the energies of conformers are calculated using the molecular mechanics method. The MMX force field was used for energy evaluations.[14]

4.3. MD Calculations. The lowest-energy geometries of **c1**, **c2**, **t1**, and **t2** from the RGS analysis (Figure 2) were selected for MD simulations using *AMBER* (version 10).[15] General AMBER force field (GAFF)[16] was used in these MD simulations for a single solute molecule (**c1**, **c2**, **t1**, or **t2**) with the standard pairwise generalized Born solvation model for implicit solvent simulations[17] in chloroform. As shown previously,[6c] GAFF MD simulations with explicit and implicit solvation of a molecule in chloroform led to similar results, while the implicit model is computationally efficient allowing long MD simulations. The AM1-BCC derived charges were used in GAFF MD calculations.[18] Simulations were of the *NVT* type. The temperature was controlled to 298 K with the Langevin algorithm. The nonbonded cutoff distance was set to 12.0 Å in MD simulations, which is either similar to or longer than those used previously.[19] After a minimization step and an equilibration for 340 ps, production runs were executed for 5 μs with a time step of 2 fs.

4.4. Quantum Mechanical Calculations. All quantum mechanical calculations were carried out using *Gaussian 09*.[20] Geometry optimizations were carried out using the M06-2X method[21] and 6-31G(d,p) basis set.[22] The M06-2X method is based on the density functional theory (DFT) and belongs to the Minnesota family of density functionals.[23] It has been shown to reproduce experimentally measured thermochemical parameters with satisfactory accuracy,[21,23] including relative stabilities of conformers in solutions.[6c] The M06-2X/6-31G(d,p) calculations also perform satisfactorily in reproducing experimentally known molecular geometries of cyclic organic molecules.[6c] The "nosymm" keyword of *Gaussian 09* was employed to carry out QM calculations with the symmetry of molecules disabled. For DFT geometry optimizations, the ultrafine numerical integration grid (with 99 radial shells and 590 angular points per shell) was used, combined with the "verytight" convergence condition (requesting the root-mean-square forces to be smaller than 1×10^{-6} hartree Bohr^{-1}). Additional frequency calculations were also undertaken in order to verify that the optimized geometries correspond to true minima, as well as for calculations of stretching frequencies and the $\Delta G_i = G_i - G_{min}$ values, where ΔG_i is the relative sum of electronic and thermal free energies and G_i and G_{min} are the sum of electronic and thermal free energies of conformer i and the lowest energy conformer, respectively (all at 298.15 K). The ΔG_i value for each conformer i was used to estimate its population p_i using

$$p_i = p_{max} e^{-\Delta G_i/RT} \quad (1)$$

where R is the universal gas constant, T is the absolute temperature (298.15 K), and p_{max} is the population of the most populated conformer.

NMR chemical shieldings and J couplings were computed at the B3LYP/6-311+G(2d,p) and B3LYP/EPR-III levels using the GIAO method.[24] Chloroform solvent effects were used in all the quantum mechanical calculations using the reaction field method, IEFPCM.[25] The satisfactory accuracy of the selected methods for the prediction of NMR parameters has been demonstrated previously.[3,4,6,26]

Conformationally averaged nuclear Overhauser effects (NOEs) from the QM calculations were determined in the following manner: (i) internuclear distances (r_i) for pairs of hydrogen atoms were calculated in each conformer i; (ii) a quantity equal to r_i^{-6} was calculated as a measure of the expected NOE in each conformer, η_i;[8] (iii) the sum of $p_i r_i^{-6}$ was used as a measure of the conformationally averaged NOE, where values of populations, p_i, were estimated using QM-predicted ΔG_i values (see eq 1 above).

Ramachandran-type histograms for MD simulations were built by using 0.5° × 0.5° bins for two dihedral angles or by using 0.025 Å × 0.5° bins for an interatomic distance and a dihedral angle. The fractional population (p_i) of each bin was calculated as the number of structures in this bin divided by the total number of structures (p_N) and multiplied by 1000.

4.5. General Experimental. All reactions were conducted in flame-dried round-bottom flasks and under a positive pressure of argon unless otherwise stated. Commercial reagents and solvents were used as received unless otherwise stated. THF was dried by being passed through a column of dry alumina. (*R*)-1-(2,2-Dimethyl-1,3-dioxolan-4-yl)-3-(trimethylsilyl)prop-2-yn-1-one (**1**) was synthesized using the method of Baker and Caddick (Scheme 1).[5] Thin layer chromatography was performed on aluminum plates precoated with silica gel 60 F_{254} and developed by exposure to a UV or potassium permanganate, or dinitrophenol, solution followed by heating. Flash chromatography was carried out on silica gel (32−70 μm). Proton and carbon NMR spectra were obtained at 600 and 151 MHz, respectively. Chemical shifts (δ) are expressed in parts per million and are referenced to the residual solvent peak. The following abbreviations are used to describe the multiplicities: s, singlet; d, doublet; t, triplet; q, quartet; m, multiplet. Gaussian resolution enhancement and zero filling were used for accurate

dx.doi.org/10.1021/jo301119h | J. Org. Chem. 2012, 77, 6290−6295

Scheme 1. Synthesis of (*R*)-4-3-(but-1-yn-1-yl)-2-(ethynyloxiran-2-yl)-2,2-dimethyl-1,3-dioxolanes 1a, 1b, 1c, and 1d

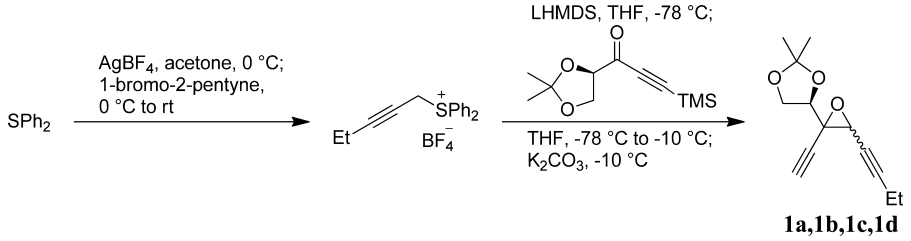

measurements of J_{HH} couplings and for the analysis of overlapping signals. Low- and high-resolution mass spectra were recorded on a double focusing magnetic sector mass spectrometer. Infrared spectra were recorded on a spectrometer operating in ATR mode. All melting points are uncorrected.

Pent-2-yn-1-yldiphenylsulfonium Tetrafluoroborate.

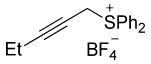

1-Bromo-2-pentyne (2.0 mL, 19.6 mmol) was added to a solution of silver tetrafluoroborate (3.6 g, 18.4 mmol) and diphenyl sulfide (20.0 mL, 119.5 mmol) in dry acetone (6 mL) in the dark at 0 °C. The reaction mixture was stirred at 0 °C for 5 min and at room temperature for 2 h. The reaction mixture was allowed to warm to room temperature, and then it was filtered and solid washed with CH_2Cl_2 (20 mL). The filtrate was concentrated in vacuo, Et_2O (80 mL) was added, and the mixture was sonicated for 5 min. The solution was filtered through a plug of Celite and the solvent removed in vacuo to produce a yellow oil. Et_2O (80 mL) was added, and the mixture was sonicated for 5 min to produce pent-2-yn-1-yldiphenylsulfonium tetrafluoroborate as a white solid (5.46 g, 16.0 mmol, 88%). Mp: 82−84 °C. ^{1}H NMR ($CDCl_3$): δ 7.89−7.91 (4H, d, J = 7.8 Hz), 7.76 (2H, t, J = 7.4 Hz), 7.70 (4H, m), 4.98 (2H, t, J = 2.4 Hz), 2.11 (2H, qt, J = 7.5, 2.4 Hz), 0.96 (3H, t, J = 7.5 Hz). ^{13}C NMR ($CDCl_3$): δ 134.9 (CH), 131.4 (CH), 131.0 (CH), 123.3 (C), 96.1 (C), 66.0 (C), 38.7 (CH_2), 13.0 (CH_3), 12.6 (CH_2). IR (neat): 3099, 3064, 2976, 2933, 2315, 2243, 2014, 1985, 1903, 1820, 1686, 1583, 1481, 1448 cm^{-1}. LRMS (CI): 253 (21%, [M − BF_4]$^+$), 187 (100), 186 (29). HMRS (CI): calcd for $C_{17}H_{17}S$ 253.1051, [M − BF_4]$^+$ 253.1045 observed.

(R)-4-3-(But-1-yn-1-yl)-2-(ethynyloxiran-2-yl)-2,2-dimethyl-1,3-dioxolane (1).

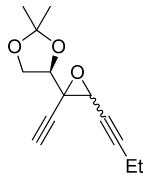

Lithium bis(trimethylsilyl)amide (800 μL, 0.80 mmol, 1 M solution in THF) was added dropwise to a suspension of pent-2-yn-1-yldiphenylsulfonium tetrafluoroborate (272 mg, 0.80-mmol) in THF (0.9 mL) at −78 °C. The reaction mixture was stirred for 15 min at −78 °C, and a solution of (*R*)-1-(2,2-dimethyl-1,3-dioxolan-4-yl)-3-(trimethylsilyl)prop-2-yn-1-one (119 mg, 0.53 mmol) in THF (1 mL) was added. The reaction mixture was stirred for 30 min at −78 °C. MeOH (1.9 mL) was added, and reaction mixture was allowed to warm rapidly to −10 °C. Potassium carbonate (155 mg, 1.12 mmol) was added, and the reaction mixture was stirred for 3 h at −10 °C. The reaction was quenched with saturated NH_4Cl at −10 °C and the mixture allowed to warm to room temperature. The aqueous phase was extracted with Et_2O (three times); the combined organic phases were washed with brine (one time), dried ($MgSO_4$), and filtered, and the solvent was removed in vacuo to produce (*R*)-4-3-(but-1-yn-1-yl)-2-(ethynyloxiran-2-yl)-2,2-dimethyl-1,3-dioxolanes **1a**, **1b**, **1c**, and **1d** as a 10.8:3.1:1.2:1 mixture of stereoisomers. Purification by column chromatography (0−5% Et_2O/petroleum ether) produced the major product, **1a**, as a single isomer and **1b**, **1c**, and **1d** as an inseparable 4.0:1.3:1.0 mixture of stereoisomers.

*Data for **1a**.* ^{1}H NMR ($CDCl_3$): δ 4.20 (1H, dd, J = 8.6, 6.8 Hz, OC*H*H), 4.09 (1H, dd, J = 8.6, 6.2 Hz, OCH*H*), 4.05 (1H, t, J = 6.4 Hz, OC*H*CH_2), 3.62 (1H, t, J = 1.6 Hz, OC*H*), 2.50 (1H, s, CC*H*), 2.26 (2H, qd, J = 7.5, 1.6 Hz, CH_2CH_3), 1.46 (3H, s, CH_3C), 1.35 (3H, s, CH_3C), 1.15 (3H, t, J = 7.5 Hz, CH_3CH_2) (see also Table S3 and Figure S11 of the Supporting Information). ^{13}C NMR ($CDCl_3$): δ 111.03 (C), 89.60 (C), 77.54 (C), 75.98 (CH), 75.48 (CH), 73.12 (C), 66.95 (CH_2), 57.79 (C), 50.11 (CH), 26.16 (CH_3), 25.27 (CH_3), 13.57 (CH_3), 12.68 (CH_3) (see also Table S4 and Figure S12 of the Supporting Information). IR (film): 3278, 2984, 2938, 2358, 2244, 2125, 1457 cm^{-1}. LRMS (EI): 205 (100%, [M − Me]$^+$), 161 (26), 91 (22), 81 (40), 66 (21), 65 (35), 63 (27), 59 (21), 53 (71), 52 (33), 51 (47). HRMS (EI): calcd for $C_{12}H_{13}O_3$ 205.0865, [M − Me]$^+$ 205.0870 observed.

*Data for **1b**, **1c**, and **1d**.* ^{1}H NMR ($CDCl_3$), mixture of 3 diastereomers with the ratio of 4.0:1.3:1.0 (**1b**:**1c**:**1d**): **1b**, δ 4.22 (1H, dd, J = 8.7, 6.2 Hz, OC*H*H), 4.18 (1H, dd, J = 8.7, 6.5 Hz, OCH*H*), 4.10 (1H, t, J = 6.3 Hz, OC*H*CH_2), 3.74 (1H, t, J = 1.7 Hz, OC*H*), 2.38 (1H, s, CC*H*), 2.25 (2H, qd, J = 7.5, 1.7 Hz, CH_2CH_3), 1.54 (3H, s, CH_3C), 1.39 (3H, s, CH_3C), 1.15 (3H, t, J = 7.5 Hz, CH_3CH_2); **1c**, δ 4.30 (1H, t, J = 6.3 Hz, OC*H*CH_2), 4.19 (1H, dd, J = 8.7, 6.6 Hz, OC*H*H), 4.06 (1H, dd, J = 8.7, 6.0 Hz, OCH*H*), 3.65 (1H, t, J = 1.6 Hz, OC*H*), 2.49 (1H, s, CC*H*), 2.26 (2H, qd, J = 7.5, 1.6 Hz, CH_2CH_3), 1.37 (3H, s, CH_3C), 1.34 (3H, s, CH_3C), 1.16 (3H, t, J = 7.5 Hz, CH_3CH_2); **1d**, δ 4.22 (1H, dd, J = 8.5, 6.9 Hz, OC*H*H), 4.12 (1H, t, J = 7.0 Hz, OC*H*CH_2), 4.01 (1H, dd, J = 8.5, 7.3 Hz, OCH*H*), 3.68 (1H, t, J = 1.7 Hz, OC*H*), 2.39 (1H, s, CC*H*), 2.22 (2H, qd, J = 7.5, 1.7 Hz, CH_2CH_3), 1.53 (3H, s, CH_3C), 1.40 (3H, s, CH_3C), 1.13 (3H, t, J = 7.5 Hz, CH_3CH_2) (see also Table S3 and Figure S13 of the Supporting Information). ^{13}C NMR ($CDCl_3$): **1b**, δ 110.86 (C), 90.36 (C), 78.67 (C), 75.20 (CH), 73.59 (CH), 72.04 (C), 66.79 (CH_2), 55.84 (C), 52.72 (CH), 26.30 (CH_3), 25.50 (CH_3), 13.43 (CH_3), 12.69 (CH_3); **1c**, δ 110.96 (C), 89.20 (C), 78.03 (C), 75.36 (CH), 75.18 (CH), 73.34 (C), 66.38 (CH_2), 57.13 (C), 49.20 (CH), 25.81 (CH_3), 25.80 (CH_3), 13.64 (CH_3), 12.68 (CH_3); **1d**, δ 110.88 (C), 89.98 (C), 78.15 (CH), 78.09 (C), 73.82 (CH), 72.13 (C), 66.13 (CH_2), 56.22 (C), 50.30 (CH), 26.36 (CH_3), 25.76 (CH_3), 13.43 (CH_3), 12.57 (CH_3) (see also Table S4 and Figure S14 of the Supporting Information). IR (film): 3279, 2984, 2934, 2882, 2239, 2124, 1740, 1457 cm^{-1}. LRMS (EI): 205 (100%, [M − Me]$^+$), 133 (43). HRMS (EI): calcd for $C_{12}H_{13}O_3$ 205.0865, [M − Me]$^+$ 205.0869 observed.

■ ASSOCIATED CONTENT

Ⓢ Supporting Information

Further results of NMR measurements (tables including experimentally measured chemical shifts and J couplings, 1D and 2D NMR spectra), MD simulations (distributions of torsional angles and interatomic distances), and QM calculations (tables including geometries and relative free energies of structures after geometry optimizations and frequency calculations, QM-predicted J couplings and chemical shifts, Cartesian coordinates of the lowest-energy conformer for each diastereomer). This material is available free of charge via the Internet at http://pubs.acs.org.

■ AUTHOR INFORMATION

Corresponding Author

*E-mail: A.E.Aliev@ucl.ac.uk.

Notes

The authors declare no competing financial interest.

■ ACKNOWLEDGMENTS

We thank University College London (UCL) for the provision of access to NMR spectrometers and computational facilities, including UCL Legion Research Computing Cluster.

■ REFERENCES

(1) (a) Günther, H. *NMR Spectroscopy*, 2nd ed.; Wiley: West Sussex, England, 1995. (b) Berger, S.; Sicker, D. *Classics in NMR Spectroscopy: Isolation and Structure Elucidation of Natural Products*; Wiley-VCH: Weinheim, Germany, 2009. (c) Bifulco, G.; Dambruoso, P.; Gomez-Paloma, L.; Riccio, R. *Chem. Rev.* **2007**, *107*, 3744. (d) Kummerlöwe, G.; Luy, B. *Annu. Rep. NMR Spectrosc.* **2009**, *68*, 194. (e) Lescheva, I. F.; Sergeyev, N. M.; Grishina, G. V.; Potapov, V. M. *Khim. Geterotsikl. Soedin.* **1986**, 1503. (f) Aliev, A. E.; Sinitsyna, A. A.; Bokanov, A. I.; Ivanov, P. Y.; Shvedov, V. I.; Kostyanovskii, R. G. *Mendeleev Commun.* **1992**, 130. (g) Bifulco, G.; Bassarello, C.; Riccio, R.; Gomez-Paloma, L. *Org. Lett.* **2004**, *6*, 1025.

(2) (a) Murphy, R. B.; Beach, M. D.; Friesner, R. A.; Ringnalda, M. N. *J. Chem. Phys.* **1995**, *103*, 1481. (b) Grimme, S. *Angew. Chem., Int. Ed.* **2006**, *45*, 4460. (c) Grimme, S.; Mück-Lichtenfeld, C. *Chirality* **2008**, *20*, 1009. (d) Aliev, A. E.; Bhandal, S.; Courtier-Murias, D. *J. Phys. Chem. A* **2009**, *113*, 10858. (e) Van Speybroeck, V.; Gani, R.; Meier, J. *Chem. Soc. Rev.* **2010**, *39*, 1764.

(3) (a) Chesnut, D. B. The Ab Initio Computation of Nuclear Magnetic Resonance Chemical Shielding. In *Reviews in Computational Chemistry*; Lipkowitz, K. B., Boyd, D. B., Eds.; John Wiley & Sons, Inc.: Hoboken, NJ, 1996; Vol. *8*, p. 245. (b) Helgaker, T.; Jaszuński, M.; Ruud, K. *Chem. Rev.* **1999**, *99*, 293. (c) *Calculation of NMR and EPR Parameters*; Kaupp, M., Bühl, M., Malkin, V. G., Eds.; Wiley-VCH: Weinheim, Germany, 2004. (d) Smith, S. G.; Goodman, J. M. *J. Am. Chem. Soc.* **2010**, *132*, 12946. (e) Atieh, Z.; Allouche, A. R.; Lazariev, A.; Van Ormondt, D.; Graveron-Demilly, D.; Aubert-Frécon, M. *Chem. Phys. Lett.* **2010**, *492*, 297.

(4) (a) Krivdin, L. B.; Contreras, R. H. *Annu. Rep. NMR Spectrosc.* **2007**, *61*, 133. (b) Bagno, A.; Saielli, G. *Theor. Chem. Acc.* **2007**, *117*, 603. (c) Helgaker, T.; Jaszuński, M.; Pecul, M. *Prog. Nucl. Magn. Reson. Spectrosc.* **2008**, *53*, 249. (d) Yongye, A. B.; Lachele Foley, B.; Woods, R. J. *J. Phys. Chem. A* **2008**, *112*, 2634. (e) Di Micco, S.; Chini, M. G.; Riccio, R.; Bifulco, G. *Eur. J. Org. Chem.* **2010**, 1411. (f) Taha, H. A.; Castillo, N. C.; Sears, D. N.; Wasylishen, R. E.; Lowary, T. L.; Roy, P.-N. *J. Chem. Theory Comput.* **2010**, *6*, 212. (g) Bally, T.; Rablen, P. R. *J. Org. Chem.* **2011**, *76*, 4818.

(5) (a) Baker, J. R.; Thominet, O.; Britton, H.; Caddick, S. *Org. Lett.* **2007**, *9*, 45. (b) Thominet, O.; Baker, J. R.; Britton, H.; Etheridge, Z. C.; Soscia, M. G.; Caddick, S. *Org. Biomol. Chem.* **2007**, *5*, 3703.

(6) (a) Aliev, A. E.; Courtier-Murias, D.; Bhandal, S.; Zhou, S. *Chem. Commun.* **2010**, *46*, 695. (b) Aliev, A. E.; Courtier-Murias, D. *J. Phys. Chem. B* **2010**, *114*, 12358. (c) Aliev, A. E.; Mia, Z. A.; Khaneja, H. S.; King, F. D. *J. Phys. Chem. A* **2012**, *116*, 1093.

(7) (a) Karplus, M. *J. Am. Chem. Soc.* **1963**, *85*, 2870. (b) Contreras, R. H.; Peralta, J. E. *Prog. Nucl. Magn. Reson. Spectrosc.* **2000**, *37*, 321.

(8) (a) Neuhaus, D.; Williamson, M. P. *The Nuclear Overhauser Effect in Structural and Conformational Analysis*, 2nd ed.; Wiley-VCH: New York, 2000. (b) Claridge, T. *High-Resolution NMR Techniques in Organic Chemistry*; Tetrahedron Organic Chemistry; Pergamon Press: Oxford, 1999; Vol. *19*.

(9) According to IUPAC nomenclature, configurations of diastereomers are (*R*)-4-[(2*S*,3*R*)-3-(but-1-yn-1-yl)-2-ethynyloxiran-2-yl]-2,2-dimethyl-1,3-dioxolane (**1a**), (*R*)-4-[(2*S*,3*S*)-3-(but-1-yn-1-yl)-2-ethynyloxiran-2-yl]-2,2-dimethyl-1,3-dioxolane (**1b**), (*R*)-4-[(2*R*,3*S*)-3-(but-1-yn-1-yl)-2-ethynyloxiran-2-yl]-2,2-dimethyl-1,3-dioxolane (**1c**), and (*R*)-4-[(2*R*,3*R*)-3-(but-1-yn-1-yl)-2-ethynyloxiran-2-yl]-2,2-dimethyl-1,3-dioxolane (**1d**).

(10) (a) Gottlieb, H. E.; Kotlyar, V.; Nudelman, A. *J. Org. Chem.* **1997**, *62*, 7512. (b) Fulmer, G. R.; Miller, A. J. M.; Sherden, N. H.; Gottlieb, H. E.; Nudelman, A.; Stoltz, B. M.; Bercaw, J. E.; Goldberg, K. I. *Organometallics* **2010**, *29*, 2176.

(11) Bax, A.; Freeman, R. *J. Am. Chem. Soc.* **1982**, *104*, 1099.

(12) Thrippleton, M. J.; Keeler, J. *Angew. Chem., Int. Ed.* **2003**, *42*, 3938.

(13) Gilbert, K. E. *PCMODEL*, version 8.5; Serena Software: Bloomington.

(14) Schlecht, M. F. *Molecular Modeling on the PC*; Wiley-VCH: New York, 1998.

(15) Case, D. A.; Darden, T. A.; Cheatham, T. E. I.; Simmerling, C. L.; Wang, J.; Duke, R. E.; Luo, R.; Crowley, M.; Ross, W. C.; Zhang, W.; Merz, K. M.; Wang, B.; Hayik, S.; Roitberg, A.; Seabra, G.; Kolossváry, I.; Wong, K. F.; Paesani, F.; Vanicek, J.; Wu, X.; Brozell, S. R.; Steinbrecher, T.; Gohlke, H.; Yang, L.; Tan, C.; Mongan, J.; Hornak, V.; Cui, G.; Mathews, D. H.; Seetin, M. G.; Sagui, C.; Babin, V.; Kollman, P. A. *AMBER10*; University of California: San Francisco, 2008.

(16) Wang, J.; Wolf, R. M.; Caldwell, J. W.; Kollman, P. A.; Case, D. A. *J. Comput. Chem.* **2004**, *25*, 1157.

(17) (a) Tsui, V.; Case, D. A. *Biopolymers* **2001**, *56*, 275. (b) Tsui, V.; Case, D. A. *J. Am. Chem. Soc.* **2000**, *122*, 2489. (c) Pellegrini, E.; Field, M. J. *J. Phys. Chem. A* **2002**, *106*, 1316.

(18) Jakalian, A.; Bush, B. L.; Jack, D. B.; Bayly, C. I. *J. Comput. Chem.* **2000**, *21*, 132.

(19) (a) Mobley, D. L.; Dumont, É.; Chodera, J. D.; Dill, K. A. *J. Phys. Chem. B* **2007**, *111*, 2242. (b) Seabra, G. M.; Walker, R. C.; Roitberg, A. E. *J. Phys. Chem. A* **2009**, *113*, 11938.

(20) Frisch, M. J.; Trucks, G. W.; Schlegel, H. B.; Scuseria, G. E.; Robb, M. A.; Cheeseman, J. R.; Scalmani, G.; Barone, V.; Mennucci, B.; Petersson, G. A.; Nakatsuji, H.; Caricato, M.; Li, X.; Hratchian, H. P.; Izmaylov, A. F.; Bloino, J.; Zheng, G.; Sonnenberg, J. L.; Hada, M.; Ehara, M.; Toyota, K.; Fukuda, R.; Hasegawa, J.; Ishida, M.; Nakajima, T.; Honda, Y.; Kitao, O.; Nakai, H.; Vreven, T.; Montgomery, J. A. Jr.; Peralta, J. E.; Ogliaro, F.; Bearpark, M.; Heyd, J. J.; Brothers, E.; Kudin, K. N.; Staroverov, V. N.; Kobayashi, R.; Normand, J.; Raghavachari, K.; Rendell, A.; Burant, J. C.; Iyengar, S. S.; Tomasi, J.; Cossi, M.; Rega, N.; Millam, N. J.; Klene, M.; Knox, J. E.; Cross, J. B.; Bakken, V.; Adamo, C.; Jaramillo, J.; Gomperts, R.; Stratmann, R. E.; Yazyev, O.; Austin, A. J.; Cammi, R.; Pomelli, C.; Ochterski, J. W.; Martin, R. L.; Morokuma, K.; Zakrzewski, V. G.; Voth, G. A.; Salvador, P.; Dannenberg, J. J.; Dapprich, S.; Daniels, A. D.; Farkas, Ö.; Foresman, J. B.; Ortiz, J. V.; Cioslowski, J.; Fox, D. J. *Gaussian 09*, revision A.02; Gaussian Inc.: Wallingford, CT, 2009.

(21) (a) Zhao, Y.; Truhlar, D. G. *Theor. Chem. Acc.* **2008**, *120*, 215. (b) Zhao, Y.; Truhlar, D. G. *J. Chem. Theory Comput.* **2008**, *4*, 1849.

(22) Ditchfield, R.; Hehre, W. J.; Pople, J. A. *J. Chem. Phys.* **1971**, *54*, 724.

(23) Peverati, R.; Truhlar, D. G. *J. Phys. Chem. Lett.* **2011**, *2*, 2810.

(24) Cheeseman, J. R.; Trucks, G. W.; Keith, T. A.; Frisch, M. J. *J. Chem. Phys.* **1996**, *104*, 5497.

(25) (a) Cances, E.; Mennucci, B. *J. Math. Chem.* **1998**, *23*, 309. (b) Cossi, M.; Rega, N.; Scalmani, G.; Barone, V. *J. Comput. Chem.* **2003**, *24*, 669.

(26) (a) Aliev, A. E.; Courtier-Murias, D. *J. Phys. Chem. B* **2007**, *111*, 14034. (b) Aliev, A. E.; Courtier-Murias, D.; Zhou, S. *THEOCHEM* **2009**, *893*, 1.